β^--delayed spectroscopy of neutron-rich tantalum nuclei: Shape evolution in neutron-rich tungsten isotopes

N. Alkhomashi,[1,*] P. H. Regan,[1] Zs. Podolyák,[1] S. Pietri,[1] A. B. Garnsworthy,[1] S. J. Steer,[1] J. Benlliure,[2] E. Caserejos,[2]
R. F. Casten,[3] J. Gerl,[4] H. J. Wollersheim,[4] J. Grebosz,[5] G. Farrelly,[1] M. Górska,[4] I. Kojouharov,[4] H. Schaffner,[4] A. Algora,[6,7]
G. Benzoni,[8] A. Blazhev,[9] P. Boutachkov,[4] A. M. Bruce,[10] A. M. Denis Bacelar,[10] I. J. Cullen,[1] L. Cáceres,[4] P. Doornenbal,[4]
M. E. Estevez,[2] Y. Fujita,[11] W. Gelletly,[1] R. Hoischen,[4,12] R. Kumar,[13] N. Kurz,[4] S. Lalkovski,[10] Z. Liu,[14] C. Mihai,[15]
F. Molina,[6] A. I. Morales,[2] D. Mücher,[9] W. Prokopowicz,[4] B. Rubio,[6] Y. Shi,[16] A. Tamii,[17] S. Tashenov,[4]
J. J. Valiente-Dobón,[18] P. M. Walker,[1] P. J. Woods,[14] and F. R. Xu[16]

[1]*Department of Physics, University of Surrey, Guildford GU2 7XH, United Kingdom*
[2]*Universidad de Santiago de Compostela, E-15706 Santiago de Compostela, Spain*
[3]*WNSL, Yale University, New Haven, Connecticut 06520, USA*
[4]*GSI, Plankstrasse 1, D-64291 Darmstadt, Germany*
[5]*The Henryk Niewodniczànski Institute of Nuclear Physics, PL-31-342 Kraków, Poland*
[6]*IFIC, CSIC-Universidad de Valencia, E-46071 Valencia, Spain*
[7]*Institute of Nuclear Research of the Hungarian Academy of Sciences, Debrecen H-4001, Hungary*
[8]*INFN, Università degli Studi di Milano, I-20133 Milano, Italy*
[9]*IKP, University of Cologne, D-50937 Cologne, Germany*
[10]*School of Environment and Technology, University of Brighton, Brighton BN2 4GJ, United Kingdom*
[11]*Department of Physics, Osaka University, Osaka, Japan*
[12]*Department of Physics, Lund University, S-22100 Lund, Sweden*
[13]*IUAC, New Delhi, India*
[14]*School of Physics and Astronomy, University of Edinburgh, Edinburgh EH9 3JZ, United Kingdom*
[15]*Horia Hulubei National Institute of Physics and Nuclear Engineering, R-76900 Bucharest, Romania*
[16]*Department of Technical Physics, Peking University, Beijing 100871, People's Republic of China*
[17]*Research Center for Nuclear Physics, Osaka University, Osaka, Japan*
[18]*INFN-Laboratori Nazionali di Legnaro, I-35020 Legnaro, Italy*
(Received 18 September 2009; published 8 December 2009)

The low-lying structure of ^{188,190,192}W has been studied following β decays of the neutron-rich mother nuclei ^{188,190,192}Ta produced following the projectile fragmentation of a 1-GeV-per-nucleon ^{208}Pb primary beam on a natural beryllium target at the GSI Fragment Separator. The β-decay half-lives of ^{188}Ta, ^{190}Ta, and ^{192}Ta have been measured, with γ-ray decays of low-lying states in their respective W daughter nuclei, using heavy-ion β-γ correlations and a position-sensitive silicon detector setup. The data provide information on the low-lying excited states in ^{188}W, ^{190}W, and ^{192}W, which highlight a change in nuclear shape at ^{190}W compared with that of lighter W isotopes. This evolution of ground-state structure along the W isotopic chain is discussed as evidence for a possible proton subshell effect for the $A \sim 190$ region and is consistent with maximization of the γ-softness of the nuclear potential around $N \sim 116$.

I. INTRODUCTION

Nuclei with $A \sim 190$ for the elements between Hf ($Z = 72$) and Pt ($Z = 78$) exhibit a wide variation of nuclear structural properties, including well-deformed prolate shapes with rotational band structures [1], K-isomeric states associated with axial symmetry in a deformed nuclear potential [2], and shape transitions across isotopic and isotonic chains [3,4]. The evolution from axially symmetric deformed prolate shapes around the valence maximum nucleus at ^{170}Dy [5] toward spherical, single-particle–like excitations close to the doubly magic nucleus ^{208}Pb is predicted to pass through a region of triaxial γ-soft and oblate nuclei [6–8]. Nuclei that are predicted to lie on the boundary between regions of prolate and oblate deformation have been described by Jolie and Linneman as prolate-oblate phase-transitional systems [9]. The phase-transitional region between axially symmetric, deformed prolate and oblate shapes is also relevant to the limits of geometric symmetry within the interacting boson model (IBM) [10–13]. Platinum isotopes with $N = 116$ and 118 represent the best cases thus far for the experimental realization of the O(6) symmetry limit of the IBM, which can be associated with a nuclear potential that is flat in the triaxial degree of freedom [14–16].

Evidence of increased γ-softness in the nuclear potential can be inferred from a number of simple experimental signatures. These signatures include a decrease in the excitation energy of the second $I^{\pi} = 2^+$ state [17] relative to the yrast $I^{\pi} = 2^+$ state and a reduction in the ratio of the excitation

TABLE I. Experimental parameters for the two FRS settings studied in the current work.

Setting	Magnetic rigidity $B\rho_1$ (Tm)	Magnetic rigidity $B\rho_2$ (Tm)	S2 degrader thickness (mg/cm^2)	S4 degrader thickness (mg/cm^2)	Beam current (p/spill)	Spill repetition (s)	Total collection time (h)
^{190}Ta	13.0805	9.5915	5050	3320	10^8	20	62
^{192}Ta	13.2285	9.7479	5050	3450	10^9	15	66

energies of the yrast $I^\pi = 4^+$ and 2^+ states, $R(4/2)$, compared to the perfect axial rotor limit of 3.33. Evidence for such behavior has been reported in a number of nuclei in this region, including ^{192}Os [18] and ^{194,196}Pt [15,19].

One focus of the current work is to extend the spectral knowledge of heavy, neutron-rich nuclei, with the specific aim of studying the predicted evolution from prolate-deformed, through γ-soft, to oblate-deformed shapes in neutron-rich tungsten ($Z = 74$) isotopes [7].

The heaviest stable tungsten isotope is ^{186}W$_{112}$. Experimental information on the neutron-rich isotopes of tungsten with $N \geqslant 116$ is sparse because of the neutron-rich nature of these systems. To investigate the change of structure with increasing neutron number and the expected evolution toward a more γ-soft and possibly oblate shape, the nuclei of interest must be studied by either deep-inelastic collisions [20–22] or projectile fragmentation reactions. Prior to this work, the heaviest even-N tungsten isotopes for which even the most rudimentary spectral information had been reported were ^{188}W and ^{190}W. In-beam spectroscopy of ^{188}W$_{114}$ was studied previously using deep-inelastic [22] and two-nucleon transfer reactions [23], which provided information on the structure of the yrast sequence up to a spin of $8\hbar$. Transitions populating the ground-state band of ^{190}W$_{116}$ were identified via isomer-delayed γ-ray spectroscopy following relativistic projectile fragmentation of a ^{208}Pb beam [24–26]. The inferred $R(4/2)$ value for ^{190}W showed a sudden decrease in value compared to the systematics in the region [24].

The present work primarily investigates the low-lying nuclear structure of ^{188}W, ^{190}W, and ^{192}W following β-delayed spectroscopy of their mother nuclei, ^{188}Ta, ^{190}Ta, and ^{192}Ta, respectively. The data confirm the previously reported $R(4/2)$ value in ^{190}W and also provide evidence for the observation of the second 2^+ state in this nucleus. The excitation energy of the yrast 2^+ state in ^{192}W is also reported for the first time in the current work. Preliminary results from this study have been reported in a series of conference papers [27–29]; this article provides the complete analysis of this work.

II. EXPERIMENTAL DETAILS

The nuclei of interest were produced following projectile fragmentation reactions between a primary beam of ^{208}Pb impinging on a natural beryllium target of thickness 2446 mg/cm^2. The 1 GeV/nucleon beam was provided by the SIS-18 heavy-ion synchrotron at GSI, Germany, with primary beam intensities of up to 10^9 ions/spill. The duration of each primary beam spill was approximately 1 s with a typical

repetition period of 15–20 s. The secondary fragmentation reaction residues were separated and identified event-by-event using the GSI Fragment Separator (FRS) [30], operated in monochromatic mode with an aluminum wedge-shaped degrader positioned in the intermediate focal plane. Two specific FRS settings were used in the current work, one centered on fully stripped (i.e., $Q = Z$) ions of ^{190}Ta and the second centered on fully stripped ^{192}Ta ions. Table I gives a summary of the experimental parameters for the FRS in these two settings.

A. Detector configuration at the FRS focal plane

A schematic of the experimental configuration used in the current work is shown in Fig. 1. The secondary ions were implanted into the RISING active stopper, which consisted of a series of double-sided silicon strip detectors (DSSSDs; see Refs. [28,31] for details). In the current work, the stopper configuration was positioned as shown in Fig. 1 and consisted of three 5 cm × 5 cm × 1 mm DSSSDs [32], each with 16 individual 3-mm-width strips on the front and back faces. The DSSSDs were used to determine the position of the implanted ion and to correlate it with its subsequent β^- decay detected in the same or neighboring pixels of the DSSSD.

The correlation of low-energy (typically hundreds of keV) β particles with significantly higher energy (typically a few GeV) implanted ions was afforded by the use of Mesytec semilogarithmic preamplifiers applied to the energy outputs of the DSSSDs [31]. These preamplifiers allowed a linear
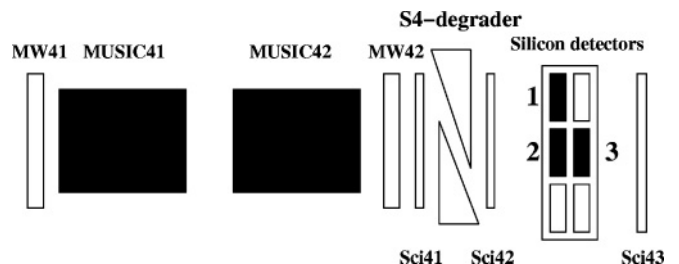

FIG. 1. Schematic of the detector configuration at the final focus of the GSI FRS for the current work. Three of the possible six positions (black boxes) in the active stopper were occupied by DSSSDs in this particular experiment. MW = multiwire position detectors; Sci = plastic scintillator detectors; MUSIC = multiple sampling ionization chamber detectors. The number 4 corresponds to the detectors being placed at the final focus (i.e., after the fourth dipole magnet) of the GSI FRS. The secondary ions are transmitted from left to right on this schematic.

amplification of the DSSSD signal for energies of up to 10 MeV, whereas a logarithmic amplification range was used for implantation energies of between 10 MeV and 3 GeV. The linear region of the preamplifier response was calibrated using the monoenergetic internal conversion electrons emitted using a standard ^{207}Bi calibration source, which yielded a measured energy full width at half maximum (FWHM) of 20 keV at 980 keV and a minimum detection threshold of approximately 150 keV. This level of electron energy resolution was used to select delayed internal conversion electron lines following decays that were observed in other FRS settings from the same experiment (for example, in the internal conversion decay of a long-lived isomer in ^{205}Au [33]). For the logarithmic portion of the preamplifier energy response, simulated signals from a pulser were used for the initial energy calibration, which was then checked by comparing the experimental data to simulations from the LISE3 code [34,35].

The active stopper was viewed by the stopped RISING γ-ray spectrometer array, which consists of 15 seven-element germanium cluster detectors with a measured total photopeak efficiency of $\sim$15% at 662 keV [36,37]. Previously, the RISING array has been used to detect γ-ray transitions emitted following the decay of isomeric states in secondary fragments produced by projectile fragmentation and fission, using the techniques described in Refs. [24,25,38–42]. This experiment represents the first time that the RISING array was also used to correlate γ-ray transitions arising from the decays of states populated following the β decay of secondary fragmentation products.

B. Data reduction and particle identification process

The identification of the projectile fragments was based on the time-of-flight (TOF) position and energy loss techniques described in Ref. [43]. The TOF in the second stage of the FRS was determined by measuring the time difference between the ions passing between two plastic scintillators mounted (i) before the degrader at the intermediate focal plane (after region S2) and (ii) at the final focal plane (after region S4). Two multiwire proportional chambers and two multiple sampling ionization chambers (MUSICs) provided position determination and energy loss information of the fragments at the final focal plane, respectively. The secondary ions of interest were then slowed down in a variable-thickness aluminum degrader (see Table I) before coming to rest in the RISING active stopper. Two plastic scintillators were placed before and after the active stopper to act as veto detectors for reactions in the final degrader and to remove events that produced light particles from nuclear reactions in the final degrader.

1. Charge-state selection of secondary ions

Charge-state anomalies in the transmitted secondary ions can cause problems with particle identification and the subsequent tagging of a β decay from specific neutron-rich isotopes. In particular, hydrogen-like (i.e., $q = Z - 1$) ions of a given element can have a similar mass-to-charge ratio, A/q, as fully stripped ($q = Z$) ions. Thus, heavier neutron-rich isotopes of the same element can cause problems in the selection process. Such so-called A/q anomalies can be partially resolved using the technique described in Ref. [43]. The difference in the magnetic rigidity of the ions, $B\rho$, before and after the intermediate focal plane degrader can be used to estimate the energy loss of the transmitted ions. This value can be correlated with the measured energy loss of the same ions in the two MUSICs at the final focus of the FRS to give loci of ions associated with different *changes* in charge state through the first and second halves of the FRS [30,37]. Niobium foils were placed after the target and the intermediate degrader to improve the atomic electron stripping efficiency. The ions transmitted through the FRS degrader were distributed into three main charge-state groups: (i) The group in which $\Delta q = 0$ is assumed to include predominantly ions that are fully stripped in both halves of the FRS. We note that there is a finite probability that the $\Delta q = 0$ condition could be satisfied by ions that are hydrogen-like in both halves of the FRS. However, the expected charge-state distributions for the ions using the GLOBAL code [44] suggest that the transmission of such events is highly suppressed compared to the fully stripped species. (ii) The group $\Delta q = +1$ is assumed to include predominantly ions that are fully stripped in the first part of the FRS and hydrogen-like ions (i.e., with one attached electron) in the second half of the FRS (i.e., after the intermediate focal plane degrader). (iii) The group $\Delta q = +2$ involves predominantly helium-like ions (two electrons) in the second half of the FRS and fully stripped in the first half. The GLOBAL code [44] gives a prediction that 96.7% of the ^{190}Ta ions were fully stripped in the first half of FRS and 81.7% in the second half. Figure 2 shows the charge-state change groups of the transmitted ions by plotting the energy loss in a MUSIC detector versus energy loss in the intermediate degrader.
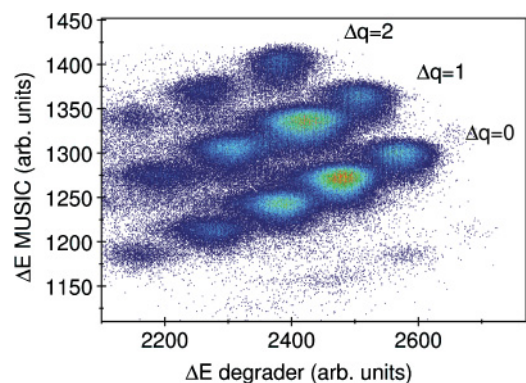

FIG. 2. (Color online) The identification of the three charge-state change groups determined using the energy loss in the intermediate degrader and the MUSIC detector at the final focal plane of the FRS. These data are taken from both the ^{190}Ta- and ^{192}Ta-centered settings. The lower group of $\Delta q = 0$ corresponds predominantly to the fully stripped charge-state transmitted through the FRS (i.e., fully stripped ions in both the first and second halves of the FRS).
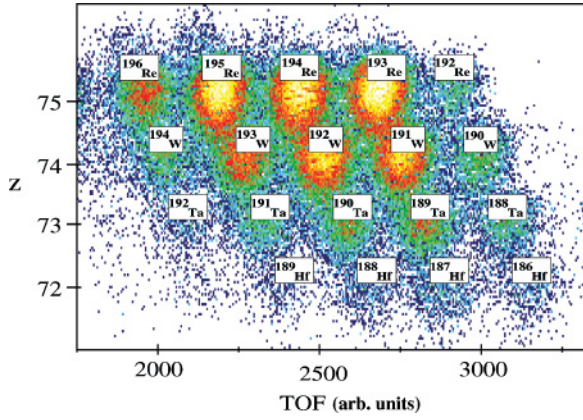
FIG. 3. (Color online) Two-dimensional particle identification plot associated with $\Delta q = 0$ (i.e., fully stripped) ions from both ^{190}Ta- and ^{192}Ta-centered settings.

2. Particle identification

The particle identification procedure was based on selecting the ions with $\Delta q = 0$, as illustrated in Fig. 2. Figure 3 shows the particle identification plot for $\Delta q = 0$ ions in terms of the atomic number, Z, as derived from the measured energy loss of the fragments in the MUSIC detector, versus the measured TOF in the second half of the FRS, which is related via the magnetic rigidity to the mass-over-charge ratio of the transmitted ions.

A two-dimensional matrix of detected γ-ray energies, as measured by the RISING array, versus their detection time relative to the signal from the heavy ion passing through the scintillation detector (Sci41) was created for all identified species in Fig. 3. The germanium γ-ray timing signal was recorded using the XIA DGF modules for each germanium channel, which gave an absolute time measurement with a resolution of 25 ns (see Refs. [37–41] for details). γ-rays from decays of previously reported isomeric states were used as internal checks on the particle identification procedure and to provide an independent validation of the γ-ray energy and timing measurement calibrations. Figure 4 shows selected γ-ray energy spectra and associated decay curves corresponding to γ-ray decays from isomeric states identified in the current work. Decays from the previously reported isomers in ^{188}Ta, ^{190}W,[1] ^{192}Re, and ^{193}Re [25] are all clearly identified.

The current data also show evidence for isomeric states in ^{187}Hf, ^{189,190}Ta, and ^{191}W. Evidence for the decays in ^{189}Ta and ^{191}W was previously reported in a conference proceeding from our Collaboration [45] following a survey of the region using the projectile fragmentation of a ^{208}Pb beam with RISING and a passive stopper. The current data confirm these observations. In addition, previously unreported isomeric decays in ^{187}Hf

---

[1]We note that the data from the current work on the isomeric decay in ^{190}W do not show any clear evidence for the 591 keV transition reported in Refs. [24,25]. This is discussed further in Ref. [26].
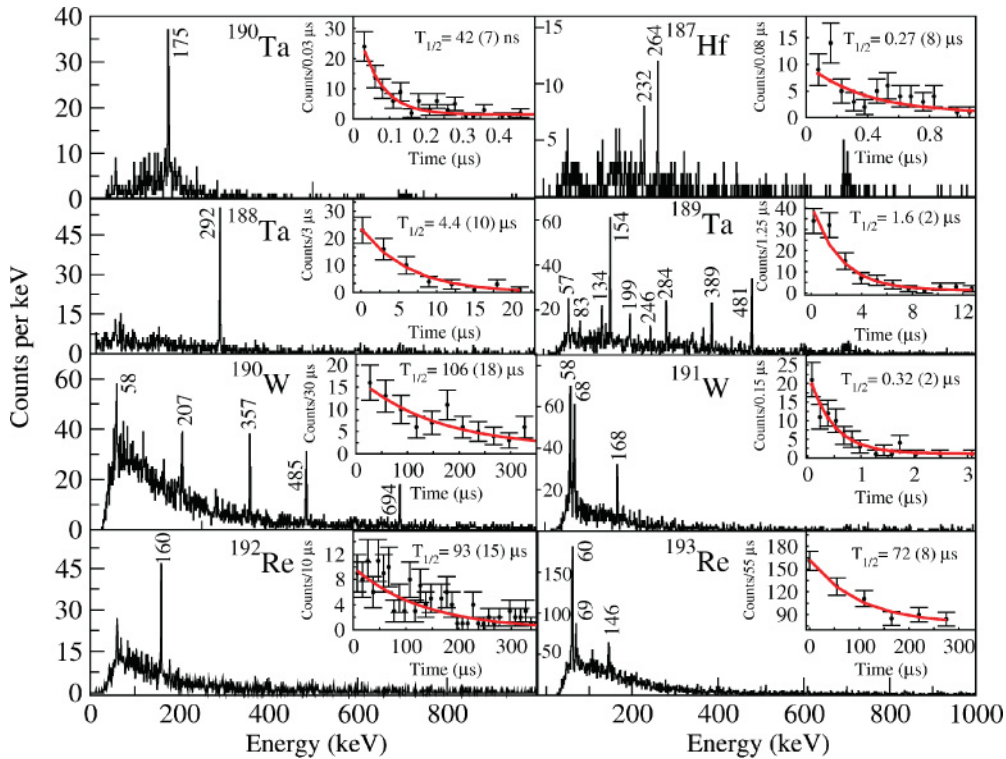

FIG. 4. (Color online) γ-ray energy and decay-time spectra of delayed events associated with isomeric states identified in ^{188,189,190}Ta ($\Delta t = 0.2 \rightarrow 22$, $0.2 \rightarrow 12$, and $0.03 \rightarrow 0.55\,\mu$s, respectively), ^{190,191}W ($\Delta t = 2 \rightarrow 395$ and $0.08 \rightarrow 3\,\mu$s, respectively), ^{192,193}Re ($\Delta t = 3 \rightarrow 350$ and $2 \rightarrow 350\,\mu$s, respectively), and ^{187}Hf ($\Delta t = 0.08 \rightarrow 1.1\,\mu$s).
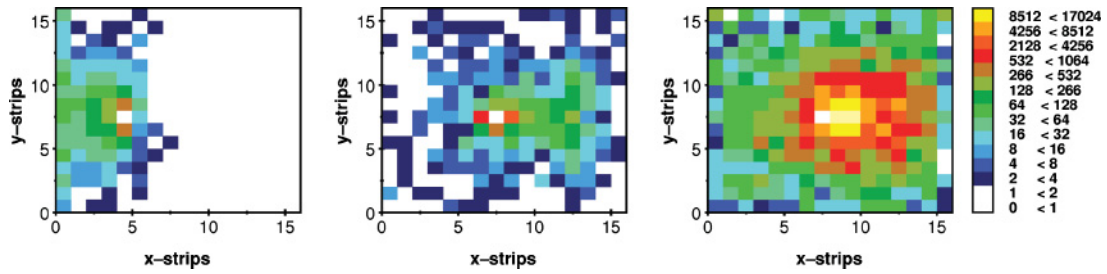
FIG. 5. (Color online) The implantion event maps for ^{188}Ta (left), ^{190}W (center), and ^{192}Re (right) as measured in the front central DSSSD from the ^{190}Ta setting.

and ^{190}Ta have been identified for the first time in the current work.

C. Implant-decay correlation technique

The technique of correlating the implanted ions with their subsequent β decay is based on the identification of the implantation position in the active stopper and the time of correlation between the implanted ion and subsequent β particle in the same or neighboring pixels of the DSSSD. The FRS was operated in monochromatic mode [46] in this experiment, which had the effect of distributing the implanted ions across a relatively wide area on the active stopper silicon detectors. This approach was required so that the probability of having multiple implantations of nuclei in the same pixel within a typical correlation time would be minimized. The use of the monochromatic mode also had the advantage of minimizing the range distribution of ions of a given species within the active stopper; thus, in general, selected isotopes of interest were stopped in a single layer of a given DSSSD. The radioactive ions were implanted in the DSSSD, with the implantation strip positions determined and an absolute measurement of the implantation time made via a digital, absolute time stamp. A valid implanted event was selected with the criterion that it produced a high-energy signal in the active stopper (>10 MeV) using the logarithmic region of the preamplifier response. Figure 5 shows two-dimensional position histograms of the implantations within one of the DSSSDs for ^{188}Ta, ^{190}W, and ^{192}Re from the ^{190}Ta setting.

The strip position, energy deposited, and time stamp for β^--decay signals in the DSSSD were correlated with the most recent implantation signal in the same or near-neighboring pixel. Figure 6 shows the energy spectrum of ions and β particles taken from the sum of energies deposited in DSSSD 1 and 2 (see Fig. 1). For each secondary ion of interest implanted in a well-defined DSSSD pixel, any energy above the threshold identified in that or neighboring pixels was considered a candidate for β^- events from the implanted mother nucleus. The time differences between the implanted events and their correlated β particle were then used to generate the β-decay time curves.

III. RESULTS

A total of 4132, 8579, and 1722 implantation events were identified for ^{188}Ta, ^{190}Ta, and ^{192}Ta ions, respectively. The

β-delayed γ rays associated with these events are shown in Fig. 7, which provides spectral information on the daughter nuclei, ^{188}W, ^{190}W, and ^{192}W. Implant-β time differences of up to 100, 30, and 15 s for ^{188}Ta, ^{190}Ta, and ^{192}Ta, respectively, were used in this analysis. These γ-ray spectra have all had random, normalized γ-ray spectra subtracted from them, with the random spectra generated from long correlation times after the implantation and normalized to the time range of the original time gate. The insets of Fig. 7 show the time spectra associated with β decays of ^{188}Ta, ^{190}Ta, and ^{192}Ta, gated on discrete γ-ray lines identified in the tungsten daughter nuclei. The quoted decay half-lives were determined using a single-component exponential decay with a least-squares-fit minimization method and assuming a constant background level. A summary of the results from this γ-ray analysis for the decays identified in ^{188}W, ^{190}W, and ^{192}W in the present work is given in Table II.

A. Decay of ^{188}Ta to ^{188}W

Figure 7(a) shows discrete transitions at γ-ray energies of 143, 297, and 434 keV following the β decay of ^{188}Ta to excited states in ^{188}W. A half-life of 19.6(20) s for this β^--decaying
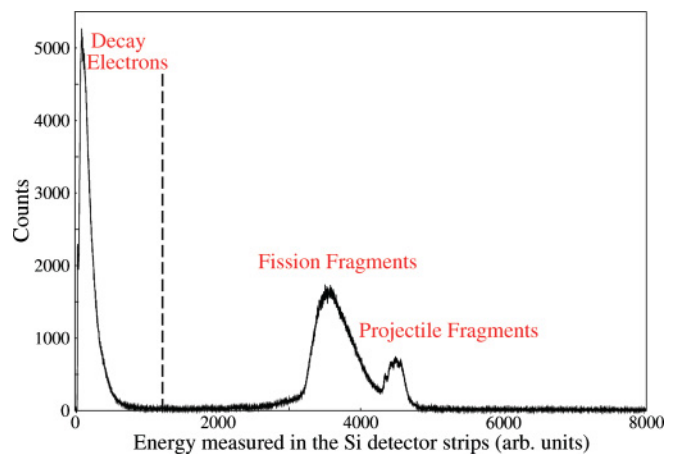

FIG. 6. (Color online) Total energy implanted by the nuclei within the silicon active stopper detector for the ^{190}Ta and ^{192}Ta settings. The double-peaked structure represents the energy deposited from both the direct implantations and for fission fragments, which are also transmitted through the FRS and pass through the active stopper. The deposited energies of β particles is shown on the left-hand side of the figure.

TABLE II. Energies, relative intensities, total internal conversion coefficient (α_{tot}), β intensities, and deduced log ft values associated with the γ-ray transitions observed in the β decay of ^{188,190,192}Ta.

Nucleus	E_{level} (keV)	E_γ (keV)	I_γ	α_{tot} [47]	I_{tot}[a]	$I_i \to I_f$	I_β (%)	log ft
^{188}Ta $\to$ ^{188}W	143	143	100(22)	1.03	203(44)	$2^+ \to 0^+$	–	–
$Q_\beta = 4854(196)$ keV	440	297	123(31)	0.09	134(35)	$4^+ \to 2^+$	–	–
	874	434	80(26)	0.04	83(26)	$6^+ \to 4^+$	53(20)	5.82(20)
^{190}Ta $\to$ ^{190}W	207	207	100(19)	0.29	129(24)	$2^+ \to 0^+$	$17(^{+21}_{-17})$	$6.3(^{+\infty}_{-0.4})$
$Q_\beta = 5634(466)$ keV	454	247	60(14)	0.16[a]	69(16)	$2_2^+ \to 2^+$	61(19)	5.65(24)
	454	454	24(10)	0.03	25(11)	$2_2^+ \to 0^+$	61(19)	5.65(24)
	564	357	30(12)	0.05	32(13)	$4^+ \to 2^+$	22(8)	6.08(23)
^{192}Ta $\to$ ^{192}W	219	219	100(26)	0.23	123(32)	$2^+ \to 0^+$	100	5.40
$Q_\beta = 6501$ keV[b]								

[a]Calculated assuming the extremum of a pure $E2$ multipolarity for the $2_2^+ \to 2_1^+$ decay.
[b]Extrapolated value, taken from Ref. [48].

state in ^{188}Ta was deduced in the current work [see the inset in Fig. 7(a)].[2]

These γ-ray energies correspond to previously observed decays from the first three excited states in the ground-state band of ^{188}W, reported following in-beam studies using both deep-inelastic reactions [22] and two-neutron transfer reactions [23]. By contrast, the transition from the yrast 8^+ state in ^{188}W ($E_\gamma = 554$ keV) as reported in Ref. [23] is not apparent in this spectrum. γ-ray energy peaks at 184, 204, and 401 keV are also identified in the β-delayed spectrum. These transitions were reported by Lane *et al.* [49] following the decay of an isomeric state in ^{188}W, with a lifetime in the 100-ns regime. The current work does not have sufficient

statistics for a γ-γ coincidence analysis of the decays from this isomer.

The log ft values were calculated assuming ground-state mass values taken from Ref. [50]. For the ^{188}Ta decay, the log ft value was estimated assuming a direct β^--feeding branch to the yrast $I^\pi = 6^+$ in ^{188}W. It should be noted, however, that the observation of discrete transitions associated with the isomer decay branch reported by Lane *et al.* suggests some degree of competition in the direct feeding through a parallel branch in ^{188}W. From the observed γ-ray intensities in Fig. 7(a), an estimate of the direct β feeding to the yrast $I^\pi = 6^+$ state has been made, which in turn has been used to extract a value for log ft for the decay of ^{188}Ta to the yrast 6^+ state in ^{188}W, given in Table II.[3] There is no evidence

_____

[2]Note that this discussion assumes that a single β-decaying state is observed in the present work. The presence of two parallel, low-lying, β-decaying states in ^{188}Ta with similar half-lives cannot be ruled out in the current work.

_____

[3]Because the complete feeding intensity into the tungsten daughter is not established in the current work, we note that the log ft values given in Table II should be regarded as lower limits rather than precise values.
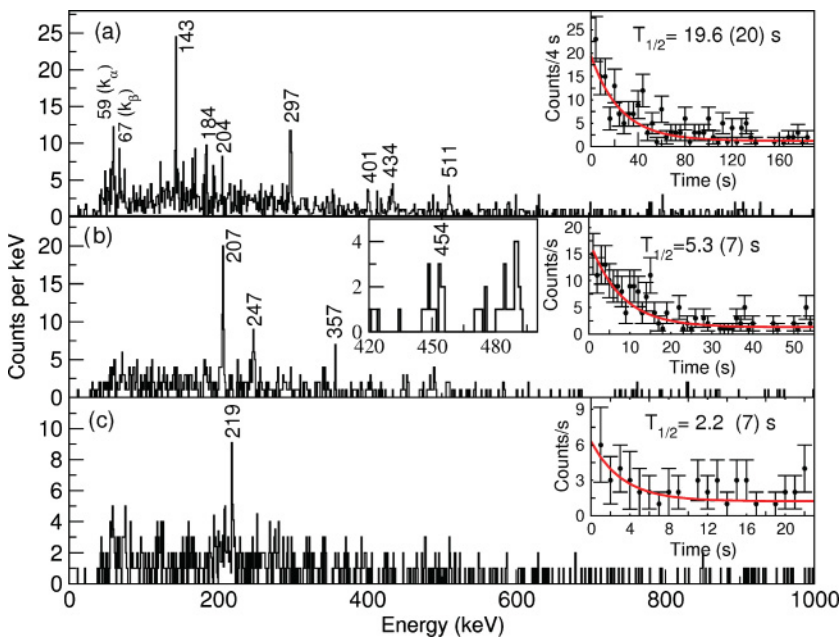

FIG. 7. (Color online) β-delayed γ-ray spectra to populate excited states in (a) ^{188}W ($\Delta t_{implant-\beta} = 100$ s); (b) ^{190}W ($\Delta t_{implant-\beta} = 30$ s), with the insert showing the enlargement of the $420 \to 500$ keV region; and (c) ^{192}W ($\Delta t_{implant-\beta} = 15$ s). A normalized random background has been subtracted from each γ-ray spectrum.

in the current work that the decays from the reported isomer feed the $I^\pi = 6^+$ yrast state in ^{188}W. Accordingly, we assume that the β^--decay feeding from the decay of ^{188}Ta leads to two parallel cascades of γ rays with 53% of direct feeding to the yrast $I^\pi = 6^+$ state and the remainder feeding to the isomeric state. Under these assumptions, it is possible to derive a lower limit for the log ft value of 5.82(20) from the direct β^--decay transition to the $I^\pi = 6^+$ state from the measured half-life of ^{188}Ta of 19.6(20) s.

B. Decay of ^{190}Ta to ^{190}W

The β-delayed γ-ray spectrum for transitions in ^{190}W is shown in Fig. 7(b). The previously reported isomeric state in ^{190}W [24–26] was also directly populated via projectile fragmentation in the current work, as shown in Fig. 4. Following population by the β^- decay of ^{190}Ta, two discrete γ-ray lines at energies of 207 and 357 keV are observed, establishing these as the decays from the yrast states with $I^\pi = 2^+$ and 4^+, respectively, in ^{190}W. A γ-γ coincidence analysis was also performed with the data from this experiment on the isomer-delayed transitions in ^{190}W, which confirmed the mutually coincident nature of the 207- and 357-keV transitions (see Fig. 8).

In addition to these previously reported transitions in ^{190}W, a transition at 247 keV is also observed in the β-delayed coincidence spectra following the decay of ^{190}Ta. This transition is interpreted as arising from the decay of the 2_2^+ state in ^{190}W, which feeds directly into the yrast $I^\pi = 2^+$ state. The limited statistics in the current β-delayed data preclude a γ-γ coincidence analysis to prove the direct feeding of the 247-keV line into the yrast $I^\pi = 2^+$ state; however, this interpretation is made on the following basis: (i) There are no other γ-ray transitions of similar intensity present in the ^{190}Ta correlated, β-delayed spectrum shown in Fig. 7(b); (ii) The 485-keV transition (which is assumed to decay from the $I^\pi = 6^+$ member of the ^{190}W ground-state band [24–26]) is not apparent in the β-decay data. (Note that the population of the yrast 6^+ state in ^{190}W is observed following the isomeric decay of the same nucleus in the current work; see Fig. 8.) Thus, it is suggested that $I^\pi = 2^+$ is the most likely spin-parity assignment for this level. (iii) An $I^\pi = 4^+$ assignment would make the 454-keV state yrast, in which case it would have been expected to have been populated in the decay of the isomeric state previously reported in ^{190}W, which it is not. An $I^\pi = 3^+$ assignment would imply that it is a collective state and built on the $I^\pi = 2^+$ bandhead of the γ-band, which can be ruled out on the basis of a lack of observation of a candidate for the required $3_\gamma^+ \to 2_2^+$ transition. (iv) Assignments of either 1^+ or 1^- at this energy in an even-even nucleus are inherently unlikely. The assumption of a 2_2^+ assignment for this state is further strengthened by the observation of a weak transition at 454 keV energy in the β-delayed spectrum for transitions in ^{190}W [see inset in Fig. 7(b)], which would represent the direct transition from the 2_2^+ state to the 0^+ ground state in ^{190}W.

The preceding arguments, together with the measured intensities (see Table II) for the observed decays from the 4^+ and 2^+ yrast states at 564 and 207 keV, respectively, in Fig. 7(b) imply a spin of $3\hbar$ for the β-decaying state in ^{190}Ta. The assumption of a spin of $3\hbar$ for the β-decaying state in ^{190}Ta is consistent (assuming direct population) with the previously discussed $I^\pi = 2^+$ assignment for the 454-keV level.

Figure 9 shows the systematics of the low-lying states in even-even tungsten isotopes with $A = 180 \to 192$ including the proposed 2_2^+ state in ^{190}W. Such states in deformed nuclei usually are associated with the bandhead of the $K^\pi = 2^+$ γ-vibrational band. We note that the assumption of the second 2^+ state in ^{190}W at an excitation energy of 454 keV is in line with the trend expected for this region, with the ongoing, systematic decrease in the energy of the 2_2^+ state relative to the yrast 4^+ states in this isotopic chain approaching the $N = 116$ isotone, ^{190}W.
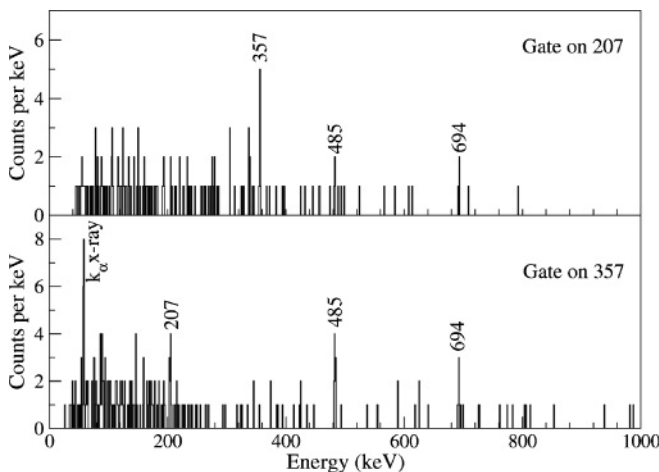

FIG. 8. Isomer-delayed γ-γ coincidence gate on (upper panel) the 207-keV transition in ^{190}W and (lower panel) the 357-keV transition in ^{190}W. The time gate condition was selected from $2 \to 395$ μs following the ion implantation in the active stopper.
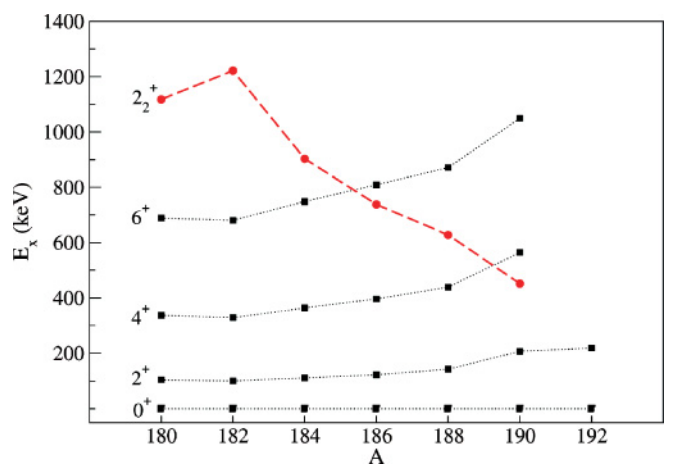

FIG. 9. (Color online) Systematic behavior of the low-lying states of even-A tungsten isotopes with $A = 180 \to 192$. The dashed lines correspond to the second $I^\pi = 2^+$ states. The data are taken from Ref. [51] and the current work.

If it is assumed that the β^- decay of the ^{190}Ta ground state feeds only the 207, 454 and 564 keV levels, then the $\log ft$ values for the β^- feeding of these levels given in Table II can be derived using the half-life measured in the present work and a Q_{β^-} value of 5.634 MeV [50].

C. Decay of ^{192}Ta to ^{192}W

The β-delayed γ-ray spectrum showing transitions in ^{192}W following the decay of ^{192}Ta is shown in Fig. 7(c). A single γ-ray line at an energy of 219 keV is evident and is interpreted as arising from the yrast $2^+ \rightarrow 0^+$ transition in ^{192}W. The decay half-life measurement for ^{192}Ta gated on the 219-keV γ-ray photopeak is 2.2 ± 0.7 s. We note that 219 keV is almost the same energy as the $2^+ \rightarrow 0^+$ transition in the $N = 118$ isotone, ^{194}Os [$E(2^+) = 218$ keV], and indeed the same, near-isospectral behavior is also evident for the $N = 116$ isotonic doublet ^{190}W and ^{192}Os [$E(2^+) \approx 207$ keV]. The possibility that the 219-keV transition observed in the present work is the result of a misassignment of the β decay of ^{194}Re into ^{194}Os can be discounted as this specific decay has also been studied in the same data set, with multiple other transitions observed resulting from decays from higher spin states in ^{194}Os [27].

The likely spin of the decaying state in the ^{192}Ta parent nucleus can be restricted to $1\hbar$ or $2\hbar$ on the basis of the expected β^--decay selection rules and the lack of any apparent line associated with the $4^+ \rightarrow 2^+$ transition in ^{192}W. However, it should be noted that, on the basis of the statistics in the current work as shown in Fig. 7(c), the possible population of higher spin states in the yrast cascade in ^{192}W and thus a higher spin for the β-decaying state cannot be ruled out. From a comparison of the number of implants and associated β^--γ-ray coincident event, there is no strong evidence of direct feeding from the β^- decay of ^{192}Ta to the ground state of ^{192}W, although such a branch cannot be exclusively ruled out in the current work. The lower limit for the $\log ft$ value for this decay given in Table II assumes 100% feeding in the β^- decay to the proposed yrast $I^\pi = 2^+$ state in ^{192}W.

IV. DISCUSSION

A. Subshell closure for the $A \sim 190$ region?

The systematics of the energy ratio $R(4/2) = E(4^+)/E(2^+)$ is arguably the best indicator of changes in low-lying nuclear structure [17]. However, for the most exotic nuclei, often only the energy of the first 2^+ state is known. In general, the energy of the first 2^+ state has been shown to decrease as the number of the valence nucleons (and related quadrupole collectivity) increases [52]. This general trend is opposite to the magnitude of the energy ratio and, thus, the $1/E(2_1^+)$ systematics should follow behavior similar to that for the $R(4/2)$ ratio. Cakirli and Casten [53] have recently used these empirically derived observables to demonstrate evidence for subshell closures in different regions of the nuclear chart. They also noted that the behavior of the $R(4/2)$ and $1/E(2_1^+)$ observables appear to scale with each other in regions of shape evolution and that evidence of subshell closures can be seen
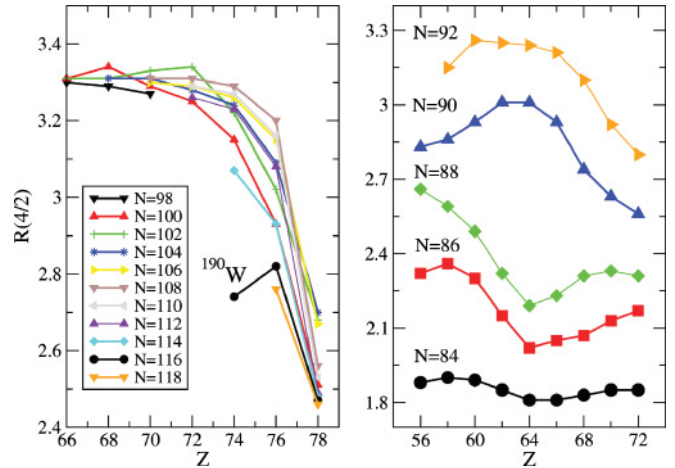

FIG. 10. (Color online) Experimental ratio of the excitation energies of the yrast $I^\pi = 4^+$ and 2^+ states [$R(4/2)$] for the even-even nuclei with (left) $Z = 66 \rightarrow 78$ and for $N > 98$ and for (right) similar plot for $Z = 56 \rightarrow 72$ and for $N = 84 \rightarrow 92$, showing the effect of the subshell closure in this region. These data are taken from Ref. [51] and the present work.

in the appearance of a "bubble" in the evolution of such plots as a function of proton or neutron number.

The energy ratios in Fig. 10 show a gradual, systematic decrease in the value of $R(4/2)$ with neutron number from ^{182}W$_{108}$ [$R(4/2) = 3.29$] to ^{188}W$_{114}$ [$R(4/2) = 3.07$]. This is followed by a very dramatic decrease at the $N = 116$ isotone, ^{190}W, for which the ratio drops to a value of $R(4/2) = 2.7$, approaching the triaxial-rotor limit of $R(4/2) = 2.5$. This gives rise to what appears to be the onset of the bubble effect described by Cakirli and Casten. With the data point for ^{192}W from the current work, this behavior is even more dramatically demonstrated by the behavior of the $1/E(2_1^+)$ observable, as shown in Fig. 11, which shows the beginning of a gap/bubble pattern for the $A \sim 190$ region. Evidence for such a subshell effect or dramatic shape evolution with the addition or removal of two nucleons can also be seen from the *difference*
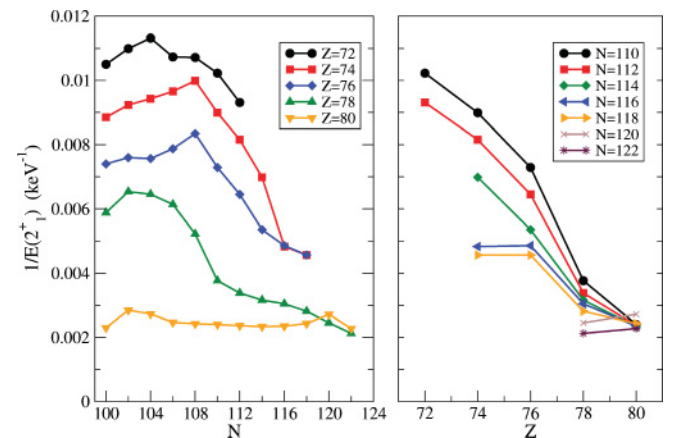

FIG. 11. (Color online) The empirical $1/E(2_1^+)$ values plotted (left) against the proton number for the $A \sim 190$ region and (right) as a function of neutron number, N, between 100 and 122. These data are taken from Ref. [51] and the present work.
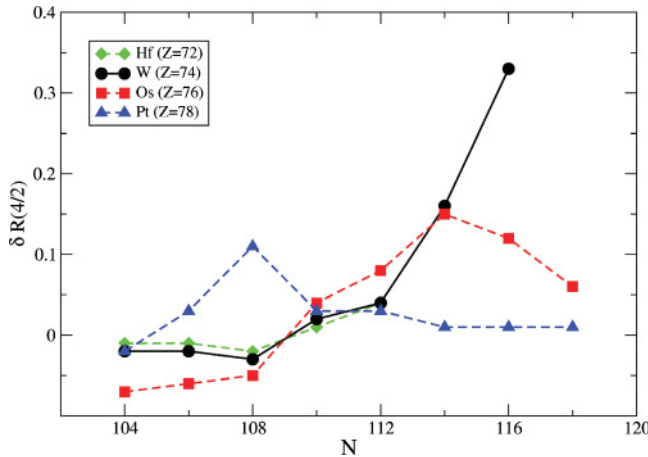
FIG. 12. (Color online) Systematics of the difference in the excitation energy ratio, $\delta R(4/2)$, for heavy even-even neutron-rich nuclei with $N = 104 \rightarrow 118$. These data are taken from Ref. [51] and the present work.

in $R(4/2)$ between neighboring even-even isotopes; that is, $\delta R(4/2) = R(4/2)_{Z,N} - R(4/2)_{Z,N-2}$ [54]. Figure 12 shows this quantity for the Hf, W, Os, and Pt isotopes with neutron numbers ranging from the midshell at $N = 104$ up to $N = 118$. The value for $\delta R(4/2)$ of greater than 0.3 between ^{188}W and ^{190}W represents one of the largest $\delta R(4/2)$ differences in the entire Segré chart. This provides compelling evidence for a dramatic change in the ground-state structure for W isotopes in going from $N = 114$ to $N = 116$.

B. Triaxial softness around $N = 116$

Evidence for triaxial (or γ-soft) collective behavior in nuclei can be obtained by using a number of basic experimental observables. These include (i) $R(2_2/2_1)$, the excitation energy ratio between the second and first spin-parity 2^+ states; (ii) the $R(4/2)$ ratio; and (iii) the ratio of the reduced matrix probabilities between the second and the first 2^+ states and from the second 2^+ state to the ground state, $R_2 = \frac{B(E2:2_2^+ \rightarrow 2_1^+)}{B(E2:2_2^+ \rightarrow 0_1^+)}$ [17]. The $E(2_1^+)$ energy is expected to increase with increasing neutron number as the $N = 126$ shell closure is approached. This increase seems to be continued for the heavier tungsten isotopes using the data for the 2_1^+ energy in the $N = 118$ isotone, ^{192}W, from the current work. This general behavior of a reduction in the energy ratio $R(4/2)$ and parallel increase in the energy of the first 2^+ state in these isotopes is indicative of the expected reduction in quadrupole collectivity as the neutron number approaches the $N = 126$ closed shell.

The $R(4/2)$ value in ^{190}W can be explained as a general feature of a γ-soft potential. Jolie and Linnemann [9] suggested that the region of nuclei between ^{180}Hf and ^{200}Hg exhibits prolate-oblate deformations and phase-shape transitions between these two shapes. There have also been theoretical predictions of a ground-state/low-lying shape transition from prolate to oblate shapes in this mass region using a variety of mean-field models (see Ref. [7] and references therein). This phase transition occurs at the O(6) symmetry in the

interacting boson approximation (IBA) [10–13]. It is useful to apply the IBA model to ^{190}W, because it allows one to investigate the γ dependence of the potential appropriate for this nucleus. To study ^{190}W, we used a simple, two-parameter IBA-1 Hamiltonian suitable for most collective nuclei. This Hamiltonian can be written as [55,56]

$$H(\zeta) = c\left[(1-\zeta)\hat{n}_d - \frac{\zeta}{4N}\hat{Q}^\chi \cdot \hat{Q}^\chi\right], \tag{1}$$

where N is the number of valence bosons, $\hat{n}_d = d^\dagger \cdot \tilde{d}$, and $\hat{Q}^\chi = (s^\dagger \tilde{d} + d^\dagger s) + \chi(d^\dagger \tilde{d})$.

This Hamiltonian has two parameters, ζ and χ, with an overall scaling factor. In this Hamiltonian, $\zeta = 0$ gives a U(5) or a quadrupole vibrator spectrum (the $\hat{n}_d$ term) while $\zeta = 1$ gives a rotor (the $\hat{Q} \cdot \hat{Q}$ term). In this latter case, one has an axial rotor for $\chi = -\frac{\sqrt{7}}{2} = -1.32$ and a γ-soft [O(6)] for $\chi = 0$. Intermediate values of ζ and χ allow one to span a wide range of collective structures.

To use Eq. (1), a technique was used based on the orthogonal cross-contour method [57]. In this approach, one can place a nucleus in the symmetry triangle for the IBA by using a contour of constant values of a pair of observables. With the data available, we used $R(4/2)$ and $E(2_2^+)$. In the O(6) limit, $E(2_2^+) = E(4_1^+)$ due to their common membership in the $\tau = 2$, O(5) multiplet. For any other situation, the IBA-1 Hamiltonian [55,56] of Eq. (1) gives $E(2_2^+) > E(4_1^+)$. Therefore, it is impossible to obtain a precise fit for the ^{190}W data, because the experimental values have $E(2_2^+) < E(4_1^+)$.

Experimentally, $R(4/2) = 2.72$ for ^{190}W. The contour for this value for $N = 9$ is shown in the inset of Fig. 13. To investigate the structure further, another observable is required, and so the $E(2_2^+)$ values are calculated along the $R(4/2) = 2.72$ contour. The results for $E(2_2^+)$ are compared with experimental value, as shown in Fig. 13.

The experimental value of $R(4/2)$ is consistent with a γ-soft [$R(4/2) \approx 2.5$] structure but does not establish it because a
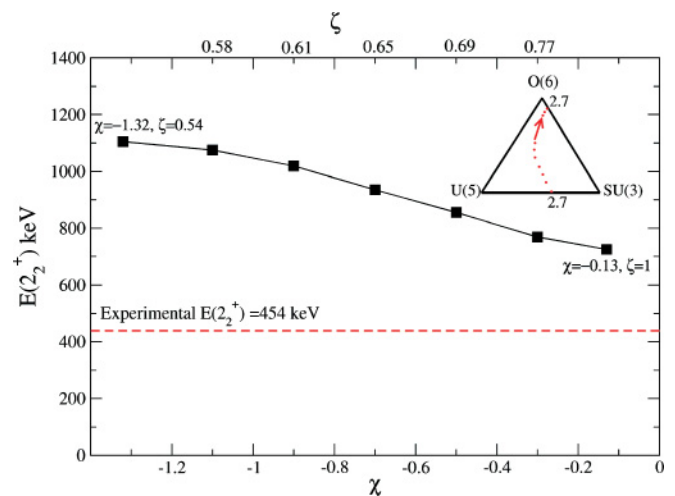

FIG. 13. (Color online) IBA-1 calculations for $E(2_2^+)$ ^{190}W along the contour in the IBA-1 symmetry triangle (dotted-line contour in the triangle) corresponding to $R(4/2) = 2.72$. The closest calculated result to the experimental $E(2_2^+)$ value is the one near the O(6) geometrically limit.
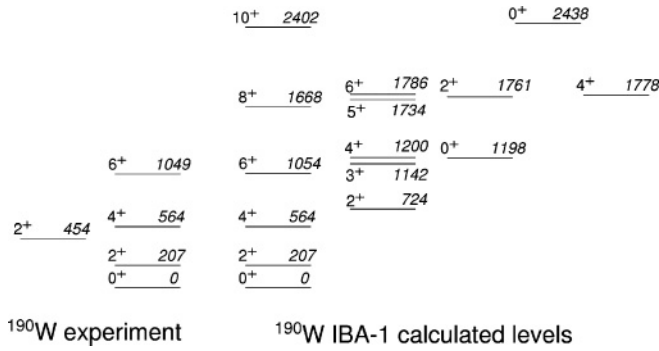
FIG. 14. Results of IBA-1 calculations for ^{190}W and comparison with the experimentally measured low-lying energy levels for this nucleus.

FIG. 16. (Color online) Empirically deduced γ values for heavy Hf $\rightarrow$ Hg even-even neutron-rich nuclei with $N = 104 \rightarrow 120$ using Eqs. (2) and (3) of the Davydov model (see text for details).

value of 2.7 can also be obtained for an axially symmetric quasirotor, as seen the inset of Fig. 13. Because the two parameters of the IBA-1 Hamiltonian of Eq. (1) cannot fit a 2_2^+ energy as low as observed experimentally, the best fit is obtained for a γ-soft structure very close to O(6). The theoretical-level scheme obtained from this procedure is compared with the experimental data in Fig. 14.

From a consideration of O(6) and also of the IBA calculations on the right-hand side of Fig. 14, one characteristic feature is a staggering in the γ-band energies, and in particular a near degeneracy of the 3_γ^+ and 4_γ^+ levels. Experimentally identifying these levels would provide a good future test of these ideas.

The identification of a weakly populated peak at 454 keV energy in ^{190}W suggests a direct transition from the 2_2^+ state to the ground state 0^+ in ^{190}W. In the pure, idealized O(6) limit, such a transition is forbidden [10–13]; however, in realistic, finite nuclear systems, such hindered transitions have been observed. The statistics in the current work preclude an angular distribution analysis to establish the $M1/E2$ mixing ratio of the proposed, unstretched $(2_2^+) \rightarrow 2_1^+$ transition in ^{190}W ($E_\gamma = 247$ keV).

Another empirical quantity, which has been used to infer the prolate-oblate shape-transition regions, is the energy ratio $E(2_2^+)/E(2_1^+)$ [58]. Figure 15 shows a systematic of this ratio versus the neutron number of even-even Hf $\rightarrow$ Hg ($Z = 72 \rightarrow 80$) isotopes $N = 104 \rightarrow 120$. The figure shows an apparent maximization of the γ softness for Os, Pt, and Hg at neutron number $N = 116$ in which the new data point for ^{190}W from the current work is consistent with this trend.

An estimate of the value of the static or average triaxial deformation parameter, γ, can be extracted from the Davydov model [59] using the energy ratio $E(2_2^+)/E(2_1^+)$. Although the Davydov model represents an asymmetric nucleus with a rigid shape, this parameter can provide a simple prediction of a static γ value that can be compared with the average γ value associated with γ-soft potentials. The expression described in
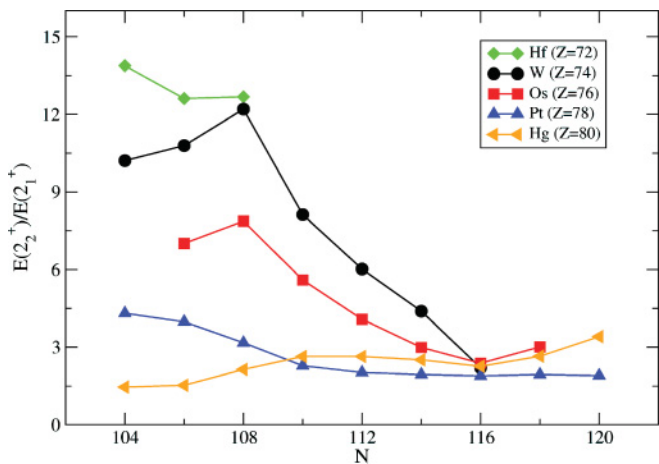

FIG. 15. (Color online) The ratio of the excitation energies of the $I^\pi = 2_2^+$ and $I^\pi = 2_1^+$ states for heavy even-even neutron-rich nuclei with $N = 104 \rightarrow 120$. These data are taken from Ref. [51] and the current work for ^{190}W.
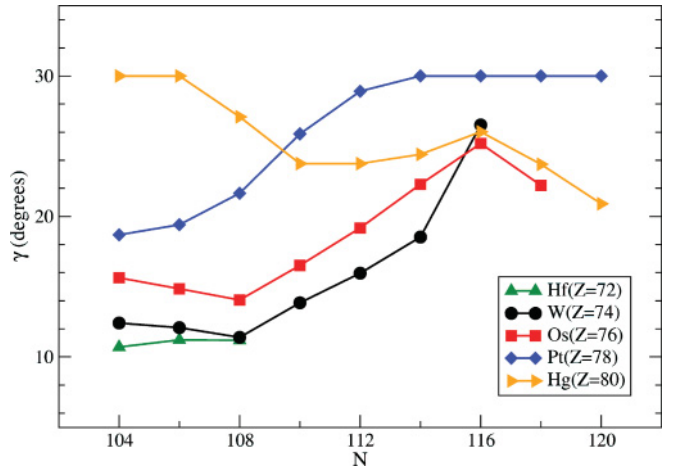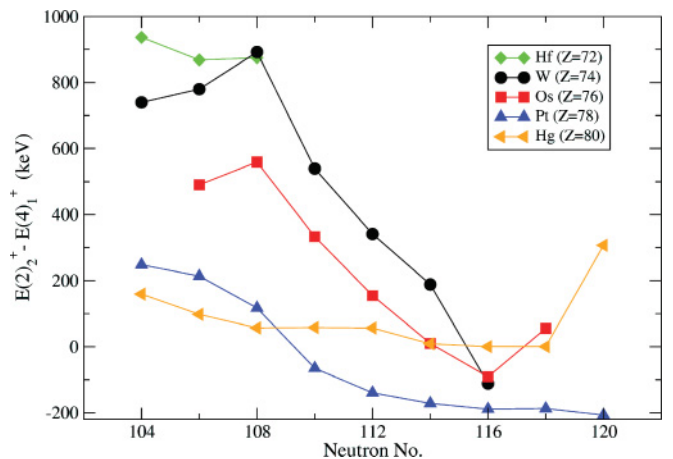

FIG. 17. (Color online) Systematics of the excitation energy difference between the $I^\pi = 2_2^+$ and $I^\pi = 4^+$ states for the even-even Hf $\rightarrow$ Hg nuclei as a function of the neutron numbers for $N = 104 \rightarrow 120$. These data are taken from Ref. [51] and the present work.
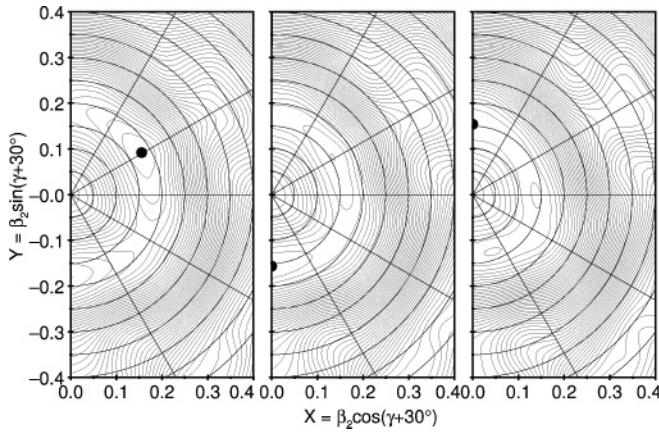
FIG. 18. (Color online) TRS calculations for the ground-state configurations of (left) ^{188}W with $\beta_2 = 0.178$ and $\gamma = 1.3°$, (middle) ^{190}W with $\beta_2 = 0.158$ and $\gamma = -120.0°$, and (right) ^{192}W with $\beta_2 = 0.136$ and $\gamma = -24.1°$. The energy contours in this figure are separated by 200 keV.

Ref. [17] is used to extract the γ value as follows:

$$\frac{E(2_2^+)}{E(2_1^+)} = \frac{[1 + X]}{[1 - X]}, \qquad (2)$$

where

$$X = \sqrt{1 - \frac{8}{9}\sin^2(3\gamma)}. \qquad (3)$$

Therefore, when $X = 1$ (i.e., for $\gamma = 0°$), the energy ratio $E(2_2^+)/E(2_1^+) \rightarrow \infty$, whereas for $X = 1/3$, $\gamma = 30°$. For ^{190}W the ratio of $E(2_2^+)/E(2_1^+)$ is equal to 2.19, leading to a value of $\gamma \approx 27°$. Figure 16 shows the γ values extracted for the even-even Hf $\rightarrow$ Hg isotopes with $N = 104 \rightarrow 120$ using Eqs. (2) and (3). The maximum γ-value appears to be reached at $N = 116$ for W, Os, and Hg.

A second quantity used to infer prolate-oblate shape-transition regions is the energy difference between the $E(2_2^+)$ and $E(4^+)$ levels [58]. According to Kumar [60], a negative value of $E(2_2^+) - E(4^+)$ (i.e., the second 2^+ state lying lower in energy than the yrast 4^+ state) is a good indicator of a region of prolate-oblate phase transition. Figure 17 shows this energy difference versus the neutron number for the region of interest. These systematics display similar characteristics to the $E(2_2^+)/E(2_1^+)$ systematics shown in Fig. 15. The neutron number $N = 116$ again appears to be associated with maximum γ softness for the low-lying states in the Os, Hg, and possibly W isotopic chains.

In their recent theoretical studies of this region using a Skyrme Hartree-Fock plus BCS pairing approach, Sarriguren *et al.* [7,61] predicted that ^{190}W lies on the near-critical point

between prolate and oblate shapes in this region, with a prediction of a very shallow triaxial minimum for the ground-state shape with a predicted $\gamma = 25°$. These authors also point out that neutron number $N = 116$ appears to be a "saddle point" for the the Yb, Hf, W, and Os isotopes with respect to maximum γ softness at the transition between axially symmetric prolate and oblate ground states for $N \leqslant 114$ and $N \geqslant 118$, respectively.

Total Routhian surface (TRS) calculations using the pre-scription described in Ref. [62] for the ground-state configurations of ^{188,190,192}W have been performed as shown in Fig. 18. The calculations predict an evolution from a prolate (albeit) γ-soft potential in ^{188}W to a very γ-soft potential for ^{190}W and ^{192}W. Indeed, the very flat energy change associated with the γ degree of freedom for $\beta_2 \approx 0.15$ can be linked to a clear predicted region of prolate/oblate shape coexistence associated with an O(6)-like potential.

V. CONCLUSIONS

The low-lying states of ^{188}W, ^{190}W, and ^{192}W have been investigated following the β^- decay of their tantalum mother nuclei populated in relativistic projectile fragmentation reactions. The results support the previously reported assignments for the first 2^+ and 4^+ states in ^{190}W and provide candidates for decays from the second 2^+ state in this nucleus and the first 2^+ state in ^{192}W. The results are consistent with the fact that $N = 116$ represents a maximum value of γ softness in this region at the intersection between prolate and oblate deformations for lighter and heavier isotopes, respectively. A direct link between the emergence of a localized proton subshell closure at $Z \leqslant 74$ for $N \geqslant 116$ and the apparent maximum values of γ softness around $N \sim 116$ is not clear at the present time.

[1] R. F. Casten, Nucl. Phys. **A443**, 1 (1985).

[2] P. M. Walker and G. Dracoulis, Nature (London) **399**, 35 (1999).

[3] C. Y. Wu *et al.*, Nucl. Phys. **A607**, 178 (1996).

[4] C. Wheldon, J. Garcés Narro, C. J. Pearson, P. H. Regan, Zs. Podolyák, D. D. Warner, P. Fallon, A. O. Macchiavelli, and M. Cromaz, Phys. Rev. C **63**, 011304 (2000).

[5] P. H. Regan, F. R. Xu, P. M. Walker, M. Oi, A. K. Rath, P. D. Stevenson *et al.*, Phys. Rev. C **65**, 037302 (2002).

[6] P. D. Stevenson, M. P. Brine, Zs. Podolyák, P. H. Regan, P. M. Walker, and J. R. Stone, Phys. Rev. C **72**, 047303 (2005).

[7] P. Sarriguren, R. Rodríguez-Guzmán, and L. M. Robledo, Phys. Rev. C **77**, 064322 (2008).

[8] Zs. Podolyák *et al.*, Phys. Rev. C **79**, 031305(R) (2009).

[9] J. Jolie and A. Linnemann, Phys. Rev. C **68**, 031301(R) (2003).

[10] F. Iachello and A. Arima, *The Interacting Boson Model* (Cambridge University Press, Cambridge, 1987).

[11] F. Iachello and A. Arima, Phys. Lett. **B53**, 309 (1974).

[12] A. Arima and F. Iachello, Phys. Rev. Lett. **40**, 385 (1978).

[13] A. Arima and F. Iachello, Phys. Rev. Lett. **35**, 1069 (1975).

[14] R. F. Casten and J. A. Cizewski, Phys. Lett. **B185**, 293 (1987).

[15] J. A. Cizewski, R. F. Casten, G. J. Smith, M. L. Stelts, W. R. Kane, H. G. Borner, and W. F. Davidson, Phys. Rev. Lett. **40**, 167 (1978).

[16] N. V. Zamfir, W.-T. Chou, and R. F. Casten, Phys. Rev. C **57**, 427 (1998).

[17] R. F. Casten, *Nuclear Structure from Simple Perspective* (Oxford University Press, Oxford, 2000), pp. 240–252.

[18] R. F. Casten, H. G. Borner, J. A. Pinston, and W. F. Davidson, Nucl. Phys. **A309**, 206 (1978).

[19] G. Berrier-Ronsin, M. Vergnes, G. Rotbard, J. Kalifa, J. Vernotte, and R. Seltz, Phys. Rev. C **23**, 2425 (1981).

[20] R. D'Alarcao *et al.*, Phys. Rev. C **59**, R1227 (1999).

[21] C. Wheldon, J. Garcés Narro, C. J. Pearson, P. H. Regan, Zs. Podolyák, D. D. Warner, P. Fallon, A. O. Macchiavelli, and M. Cromaz, Phys. Rev. C **63**, 011304(R) (2000).

[22] Zs. Podolyák *et al.*, Int. J. Mod. Phys. E **13**, 123 (2004).

[23] T. Shizuma *et al.*, Eur. Phys. J. A **30**, 391 (2006).

[24] Zs. Podolyák *et al.*, Phys. Lett. **B491**, 225 (2000).

[25] M. Caamano *et al.*, Eur. Phys. J. A **23**, 201 (2005).

[26] G. F. Farrelly *et al.*, Acta Phys. Pol. B **40**, 885 (2009).

[27] P. H. Regan *et al.*, AIP Conf. Proc. **1090**, 122 (2008).

[28] P. H. Regan *et al.*, Int. J. Mod. Phys. E **17**, 8 (2008).

[29] N. Alkhomashi *et al.*, Acta Phys. Pol. B **40**, 875 (2009).

[30] H. Geissel *et al.*, Nucl. Instrum. Methods Phys. Res. B **70**, 286 (1992).

[31] R. Kumar *et al.*, Nucl. Instrum. Methods Phys. Res. A **598**, 754 (2009).

[32] Micron Semiconductor Ltd, Marlborough Road, Lancing Sussex, England, http://www.micronsemiconductor.co.uk (2009).

[33] Zs. Podolyák *et al.*, Phys. Lett. **B672**, 116 (2009).

[34] D. Bazin, O. Tarasov, M. Lewitowicz, and O. Sorlin, Nucl. Instrum. Methods Phys. Res. A **482**, 307 (2002).

[35] O. B. Tarasov and D. Bazin, Nucl. Phys. **A746**, 411 (2004).

[36] S. Pietri *et al.*, Nucl. Instrum. Methods Phys. Res. B **261**, 1079 (2007).

[37] S. Pietri *et al.*, Acta Phys. Pol. B **38**, 1255 (2007).

[38] A. B. Garnsworthy *et al.*, Phys. Lett. **B660**, 326 (2008).

[39] S. J. Steer *et al.*, Phys. Rev. C **78**, 061302(R) (2008).

[40] D. Rudolph *et al.*, Phys. Rev. C **78**, 021301(R) (2008).

[41] M. Gorska *et al.*, Acta Phys. Pol. B **38**, 1219 (2007).

[42] L. Caceres *et al.*, Phys. Rev. C **79**, 011301(R) (2009).

[43] J. Benlliure, K.-H. Schmidt, D. Cortina-Gil, T. Enqvist, F. Farget, A. Heinz, A. R. Junghans, J. Pereira, and J. Taieb, Nucl. Phys. **A660**, 87 (1997).

[44] C. Scheidenberger, Th. Stöhlker, W. E. Meyerhof, H. Geissel, P. H. Mokler, and B. Blank, Nucl. Instrum. Methods Phys. Res. B **142**, 441 (1998).

[45] S. J. Steer *et al.*, Int. J. Mod. Phys. E **18**, 1002 (2009).

[46] G. Münzenberg, Nucl. Instrum. Methods Phys. Res. B **70**, 265 (1992).

[47] T. Kibédi, T. W. Burrows, M. B. Trzhaskovskaya, P. M. Davidson, and C. W. Nestor Jr., Nucl. Instrum. Methods Phys. Res. A **589**, 202 (2008).

[48] P. Möller, J. R. Nix, W. D. Myers, and W. J. Swiatecki, At. Data Nucl. Data Tables **59**, 185 (1995).

[49] G. Lane *et al.* (private communication, 2009).

[50] G. Audi, A. H. Wapstra, and C. Thibault, Nucl. Phys. **A729**, 337 (2003).

[51] Evaluated Nuclear Structure Data File, ENSDF, online database, National Nuclear Data Center, 2008.

[52] R. F. Casten and N. V. Zamfir, Phys. Rev. Lett. **70**, 402 (1993).

[53] R. B. Cakirli and R. F. Casten, Phys. Rev. C **78**, 041301(R) (2008).

[54] R. B. Cakirli and R. F. Casten (private communication, 2009).

[55] V. Werner, N. Pietralla, P. von Brentano, R. F. Casten, and R. V. Jolos, Phys. Rev. C **61**, 021301(R) (2000).

[56] P. O. Lipas, P. Toivonen, and D. D. Warner, Phys. Lett. **B155**, 295 (1985).

[57] E. A. McCutchan and R. F. Casten, Phys. Rev. C **74**, 057302 (2006).

[58] R. F. Casten, A. I. Namenson, W. F. Davidson, D. D. Warner, and H. G. Borner, Phys. Lett. **B76**, 280 (1978).

[59] A. S. Davydov and G. F. Filippov, Nucl. Phys. **8**, 237 (1958).

[60] K. Kumar, Phys. Rev. C **1**, 369 (1970).

[61] L. M. Robledo, R. Rodríguez-Guzmán, and P. Sarriguren, J. Phys. G: Nucl. Part. Phys. **36**, 115104 (2009).

[62] F. R. Xu, Phys. Lett. **B435**, 257 (1998).